

Power System Electromagnetic Transient Stability: an Analysis Based on Convergent Hamiltonian

Xinyuan Jiang, Constantino M. Lagoa, and Yan Li

Abstract—Transient stability is crucial to the reliable operation of power systems. Existing theories rely on the simplified electromechanical models, substituting the detailed electromagnetic dynamics of inductor and capacitor with their impedance representations. However, this simplification is inadequate for the growing penetration of fast-switching power electronic devices. Attempts to extend the existing theories to include electromagnetic dynamics lead to overly conservative stability conditions. To tackle this problem more directly, we study the condition under which the power source and dissipation in the electromagnetic dynamics tend to balance each other asymptotically. This is equivalent to the convergence of the Hamiltonian (total stored energy) and can be shown to imply transient stability. Using contraction analysis, we prove that this property holds for a large class of time-varying port-Hamiltonian systems with (i) constant damping matrix and (ii) strictly convex Hamiltonian. Then through port-Hamiltonian modeling of the electromagnetic dynamics, we obtain that the synchronized steady state of the power system is globally stable if it exists. This result provides new insights into the reliable operation of power systems. The proposed theory is illustrated in the simulation results of a two-machine system.

Index Terms—Transient stability analysis, contraction analysis, port-Hamiltonian system, electromagnetic dynamics, limit cycle

I. INTRODUCTION

TRANSIENT stability is crucial to the planning and operation of power systems and has become even more so with the increasing penetration of power electronic technologies, whose dynamics are dependent primarily on their local controls. These local controls operate on the electromagnetic time scale from 1 μ s to 1 ms, which necessitates more detailed analyses into the transient dynamics of power systems in the electromagnetic time scale [1]. In addition to the increased complexity in the types of dynamic agents involved, there is also a growing trend of individual generators for industrial and commercial power systems to sustain islanding situations during blackouts and to sell power to the bulk power system during normal operation [2]. This creates increased complexity in the loading and configuration, which magnifies the limitations of the existing methods for transient stability analysis. There are mainly four types of methods for analyzing transient stability, namely, angle stability, feedback linearization, passivity, and direct methods.

Firstly, angle stability [2], [3] aims at monitoring the torque angles of every synchronous generator in the system to detect whether some generators are entering into stable or unstable

swing post fault. It relies on the observation that if the angles do not exceed the limits of the power-angle curves, in out-of-step conditions [4], then the restoring and damping torque cause the angles to synchronize. The limitation, however, is that it does not study the system dynamics directly, but aims to extract patterns from numerical simulations of instability. Therefore, it does not provide enough insight into the effects of the controls.

Secondly, feedback linearization can algebraically linearize and decouple the interactions between the generators and the loads to obtain linear subsystems which are suitable for linear control. In [5], an synchronous generator excitation control is designed to guarantee transient stability of the simplified multimachine power system model. In [6], a microgrid secondary control is designed for improving the tracking performance for frequency and voltage. However, the limitation is that the electromagnetic dynamics usually cannot be fully linearized so that only partial stability can be attained.

Thirdly, passivity is a distributed subsystem-level property for verifying overall transient stability. It is closely related to physical energy dissipation, and so it can handle systems with nonzero line conductance [7], [8]. The main issue in its application to transient stability is that the nonlinear transformations between different dq -reference frames of the generators is a major obstacle for verifying passivity [9].

Last but not least, the direct method for transient stability analysis [10]–[13] consists of (i) a model of the power system with simplifications, and (ii) the associated energy function (a function of voltage angles and frequencies), which decreases in time monotonically. Under certain conditions, the energy function becomes locally a Lyapunov function, but their differences are seen from the following aspects:

- To define the energy function, the periodic angle domain is unrolled into a real domain.¹ This explains why the input power, which is non-conservative, can seemingly be “integrated” to get a linear function of the unrolled angles, i.e.,

$$\int P_m \Delta\omega dt = P_m \delta.$$

Then, by designating a reference bus of 0 voltage angle, the steady state becomes an isolated equilibrium point.²

¹We mean that the 2π equivalence of the domain \mathbb{T}^n is removed so that two equivalent angle vectors in \mathbb{T}^n as their difference is multiples of 2π are no longer deemed equivalent [14], [15].

²If a reference bus is not chosen, the system has angle symmetry, which causes a set of equilibrium points whose angles are rigidly shifted. To deal with this problem, usually a reference angle rotating at the average frequency is chosen [10]. However, this does not work without the constant impedance assumption.

- The stability of the equilibrium point is not implied from the energy function because of its boundedness. Instead, given that this equilibrium point is locally asymptotically stable,³ an estimated region of attraction can be obtained by calculating the values of the energy function at those unstable equilibrium points located on the boundary of the region of attraction. Then the minimum of the function values is used for estimating the critical clearing time for a fault given the post-fault initial condition [13].

The limitation of the direct method, which prevents its wider application, is the difficulty in finding the unstable equilibrium points on the boundary of the region of attraction. It is worth noting that the estimated region of attraction from the direct method is unbounded [11] compared to the bounded estimate from angle stability [2].

An important limitation that is shared by almost all existing methods is that they inadvertently focus on the slower electromechanical dynamics. In an electromechanical model, the dynamics of the inductors and capacitors are replaced by the impedance value at a certain frequency. In contrast, in the full-order equations for the inductor and capacitor in (28) and (27) in a stationary reference frame, there is a lack of frequency-dependent terms. This is because the steady-state frequency, in fact, an incidence of an energy balance in the system. For example, the value of the steady-state frequency changes as soon as the load is changed slightly. Therefore, based on the electromagnetic model, the equilibrium of the system is not an equilibrium point, but rather an energy-balancing limit cycle. If an infinite bus is present, the frequency of the limit cycle is equal to the frequency of the infinite bus. If an infinite bus is not present, the frequency of the limit cycle is determined autonomously.

By viewing the power system transient stability problem as checking the ability of the system to reach a certain energy balance, it is reasonable to ask the question: *Whether there is a certain class of systems such that its Hamiltonian (total stored energy) is convergent to the same value (not necessarily zero) along every solution?*

It will be shown in this paper that the answer to the above question is affirmative. In particular, the class of time-varying port-Hamiltonian system with constant damping matrix and strictly convex Hamiltonian verifies that the Hamiltonian along every trajectory converges to the same value (the converging Hamiltonian principle in Proposition 4). It is implied from a more fundamental property called contraction in the quotient space, which is developed first in Section III. Then, by modeling the electromagnetic dynamics of the power system as a time-varying port-Hamiltonian system in Section IV, we obtain convergence of the Hamiltonian, which combined with the constant (not depending on the state) network structure of the power system yields the global attractivity of the limit cycle. Finally, in Section V, electromagnetic simulation of a two-machine power system from random initial conditions confirms the theoretical results, and the existence of a synchronized limit cycle is identified as the main challenge in

operating AC power systems. The contributions of this paper are summarized as follows:

- The global attractivity of the limit cycle steady state of the electromagnetic power system model is proved based on the converging Hamiltonian principle. The compositional feature of the method provides a general framework for cooperation of synchronous generator and power electronics control.
- A large class of time-varying port-Hamiltonian system is proved to be contractive in a special quotient space. Only the constant positive-definiteness of the damping matrix and the strict convexity of the Hamiltonian are assumed, which enables its wider application.
- The numerical example shows that several instability concepts in power engineering are related to the nonexistence of a synchronized limit cycle, rather than related to the non-attraction of its orbit.

Notation: The imaginary unit is j . A vector of zeros is 0_n . A vector of ones is 1_n . Their subscripts are usually omitted when the dimension is clear. The transpose of a matrix is \mathbf{A}^\top ; the Hermitian transpose is \mathbf{A}^H . For a matrix \mathbf{A} in an inner product space, the adjoint is \mathbf{A}^* . The symbol $\text{col}(\mathbf{x}_i)$ denotes a column vector that stacks the vectors \mathbf{x}_i for $i = 1, \dots, n$. The complex vector space \mathbb{C}^n we consider in this paper is equivalent to the \mathbb{R}^{2n} considering the mapping

$$\mathcal{U} : \mathbf{x} \mapsto \hat{\mathbf{x}} = \text{col}([\Re \mathbf{x}_i, \Im \mathbf{x}_i]^\top).$$

The derivative of real-valued functions defined on \mathbb{C}^n are taken after mapping them to the equivalent real function. For $\mathbf{f} : \mathbb{C}^n \rightarrow \mathbb{C}^n$, the real Jacobian $D\mathbf{f}(\mathbf{x})$ is the Jacobian of $\mathbf{f}(\mathcal{U}^{-1}(\hat{\mathbf{x}}))$. For $H : \mathbb{C}^n \rightarrow \mathbb{R}$, the real Hessian $D^2H(\mathbf{x})$ is the Hessian of $H(\mathcal{U}^{-1}(\hat{\mathbf{x}}))$. An exception is the complex gradient. For the inner product $\langle \mathbf{z}, \mathbf{x} \rangle = \Re\{\mathbf{z}^H \mathbf{x}\}$, the complex gradient is defined, for $H : \mathbb{C}^n \rightarrow \mathbb{R}$, as $\nabla H(\mathbf{x}) = 2 \text{col}(\frac{\partial H}{\partial x_i^*})$, where $\frac{\partial H}{\partial x_i^*}$ is the Wirtinger derivative [17]. The complex gradient allows us to replace a direction derivative by an inner product:

$$\frac{\partial}{\partial \mathbf{x}} H(\mathbf{x}) \cdot \mathbf{v} = \Re\{\nabla H(\mathbf{x})^H \mathbf{v}\}.$$

II. BACKGROUND

In this section, we discuss the background for the main theoretical development in Section III: the contraction property implied from the port-Hamiltonian structure of a nonlinear time-varying (NLTV) system. We introduce this background knowledge by reviewing standard results on contraction of a general NLTV system, and contraction of a port-Hamiltonian NLTV system. We highlight the conservativeness of the standard results to motivate the more involved theoretical development in Section III.

A. Standard Contraction Definition

Consider the NLTV system $\dot{\mathbf{x}} = \mathbf{f}(t, \mathbf{x})$ for $t \in \mathbb{R}$ and $\mathbf{x} \in \mathbb{D}$, for an invariant set $\mathbb{D} \subset \mathbb{C}^n$ such that, at each $\mathbf{x} \in \mathbb{D}$, the tangent space⁴ is $T_{\mathbf{x}}\mathbb{D} = \mathbb{C}^n$ with the inner product

$$\langle \mathbf{y}, \mathbf{x} \rangle = \Re\{\mathbf{y}^H \mathbf{P} \mathbf{x}\}, \quad (1)$$

³Without this condition, it is almost impossible to establish that the region of attraction is nonempty. See the same idea used later in [16].

⁴The tangent space $T_{\mathbf{x}}\mathbb{D}$ of a manifold \mathbb{D} at \mathbf{x} is the collection of tangent vectors of smooth curves in \mathbb{D} that passes through \mathbf{x} ; see [18, Def. 3.33].

where $\mathbf{P} \in \mathbb{C}^{n \times n}$ is Hermitian positive-definite. This inner product verifies the inner product axioms for the vector space \mathbb{C}^n with the field \mathbb{R} . The associated norm is

$$\|\mathbf{x}\| = \sqrt{\langle \mathbf{x}, \mathbf{x} \rangle} = \sqrt{\Re\{\mathbf{x}^H \mathbf{P} \mathbf{x}\}}.$$

We choose to work with the space \mathbb{C}^n instead of the equivalent real space \mathbb{R}^{2n} because complex variables readily represent amplitudes and angles in models of the power system.

Contraction of the NLTV system is a sufficient condition for stability that requires two solutions from any two initial conditions to converge exponentially to each other in terms of the norm of their difference in time. The contraction property is particularly useful in stability analysis in that the global condition can be checked locally with the Jacobian matrix $D\mathbf{f}(t, \mathbf{x})$: the NLTV system is said to be infinitesimally contracting if, for some $c > 0$ (the contraction rate),

$$\langle \delta, D\mathbf{f}(t, \mathbf{x})\delta \rangle \leq -c\langle \delta, \delta \rangle, \quad (2)$$

for all $t \in \mathbb{R}$ and $\delta \in T_{\mathbf{x}}\mathbb{D} = \mathbb{C}^n$. It is not hard to prove that if the domain \mathbb{D} is convex, then infinitesimal contraction implies global contraction [19], [20]; that is, for every $\mathbf{x}_1, \mathbf{x}_2 \in \mathbb{D}$ and $t_0 \in \mathbb{R}$, the condition (2) implies

$$\|\Phi(t, t_0, \mathbf{x}_1) - \Phi(t, t_0, \mathbf{x}_2)\| \leq e^{-c(t-t_0)} \|\mathbf{x}_1 - \mathbf{x}_2\| \quad (3)$$

where $\Phi(t, t_0, \mathbf{x}_0)$ is the solution of the NLTV system from the initial condition (t_0, \mathbf{x}_0) . The contraction condition (2) depends critically on the inner product chosen. Let us examine the condition (2) in more detail.

For every matrix $\mathbf{A} \in \mathbb{C}^{n \times n}$, the matrix measure is defined as⁵

$$\mu(\mathbf{A}) = \sup_{\delta \in \mathbb{C}^n \setminus \{0\}} \frac{\langle \delta, \mathbf{A}\delta \rangle}{\langle \delta, \delta \rangle}. \quad (4)$$

From this definition, the contraction condition (2) is equivalently expressed as $\mu(D\mathbf{f}(t, \mathbf{x})) \leq -c$. Since the skew-adjoint part of \mathbf{A} yields zero in the numerator of (4), $\mu(\mathbf{A})$ is equal to

$$\mu(\mathbf{A}) = \sup_{\delta \in \mathbb{C}^n \setminus \{0\}} \frac{\langle \delta, \frac{1}{2}(\mathbf{A} + \mathbf{A}^*)\delta \rangle}{\langle \delta, \delta \rangle} \quad (5)$$

The adjoint \mathbf{A}^* is a mapping such that $\langle \mathbf{x}, \mathbf{A}\mathbf{y} \rangle = \langle \mathbf{A}^*\mathbf{x}, \mathbf{y} \rangle$; see [22, Sec. 4.4]. For the inner product (1), the adjoint of \mathbf{A} is obtained as $\mathbf{P}^{-1}\mathbf{A}^H\mathbf{P}$, which we substitute into (5) to get

$$\begin{aligned} \mu(\mathbf{A}) &= \sup_{\delta \in \mathbb{C}^n \setminus \{0\}} \frac{\Re\{\delta^H \mathbf{P} \frac{1}{2}(\mathbf{A} + \mathbf{P}^{-1}\mathbf{A}^H\mathbf{P})\delta\}}{\Re\{\delta^H \mathbf{P} \delta\}} \\ &= \sup_{\delta \in \mathbb{C}^n \setminus \{0\}} \frac{\Re\{\frac{1}{2}\delta^H(\mathbf{P}\mathbf{A} + \mathbf{A}^H\mathbf{P})\delta\}}{\Re\{\delta^H \mathbf{P} \delta\}} \\ &= \sup_{s \in \mathbb{C}^n \setminus \{0\}} \frac{\Re\{\frac{1}{2}s^H \mathbf{P}^{-\frac{1}{2}}(\mathbf{P}\mathbf{A} + \mathbf{A}^H\mathbf{P})\mathbf{P}^{-\frac{1}{2}}s\}}{\Re\{s^H s\}}, \end{aligned}$$

where $s = \mathbf{P}^{\frac{1}{2}}\delta$. We then obtain the following expression for the matrix measure that is dependent on the matrix \mathbf{P} :

$$\mu(\mathbf{A}) = \lambda_{\max} \left\{ \frac{1}{2} \mathbf{P}^{-\frac{1}{2}} (\mathbf{P}\mathbf{A} + \mathbf{A}^H\mathbf{P}) \mathbf{P}^{-\frac{1}{2}} \right\}.$$

⁵The matrix measure is commonly defined in terms of a vector norm [21] or in terms of an inner product. The latter is more appropriate for port-Hamiltonian systems, which are naturally defined in inner product spaces.

By [23, Thm. 4.6], if \mathbf{A} is Hurwitz, there exist (many) \mathbf{P} 's and the associated inner products such that $\mu(\mathbf{A}) < 0$. However, not all \mathbf{P} 's and such inner products verify $\mu(\mathbf{A}) < 0$.

In dealing with the general NLTV systems, the skew-adjoint part of the Jacobian matrix is ignored in order to check contraction. The skew-adjoint part can usually be related to the energy-preserving or structural part of the dynamics; this part is explicitly separated from the energy-dissipating or damping part in the port-Hamiltonian formulation of NLTV systems.

B. Port-Hamiltonian System

In this paper, we consider the input-state-output port-Hamiltonian (pH) system with a constant damping matrix:

$$\Sigma : \begin{cases} \dot{\mathbf{x}} = (\mathbf{J}(t, \mathbf{x}) - \mathbf{R})\nabla_{\mathbf{x}}H(t, \mathbf{x}) + \mathbf{G}\mathbf{u} \\ \mathbf{y} = \mathbf{G}^H\nabla_{\mathbf{x}}H(t, \mathbf{x}) \end{cases} \quad (6)$$

In (6), $\mathbf{x} \in \mathbb{C}^n$ is the state vector, $\mathbf{u} \in \mathbb{C}^m$ and $\mathbf{y} \in \mathbb{C}^m$ are the input and output vectors, $\mathbf{J}(t, \mathbf{x}) \in \mathbb{C}^{n \times n}$ is the time-varying interconnection matrix that is skew-Hermitian, $\mathbf{R} \in \mathbb{C}^{n \times n}$ is the constant damping matrix, $\mathbf{G} \in \mathbb{C}^{n \times m}$ is the input matrix, $H(t, \mathbf{x}) \geq 0$ is the time-varying Hamiltonian, and $\nabla_{\mathbf{x}}H(t, \mathbf{x})$ is the complex gradient with respect to the inner product $\langle \mathbf{y}, \mathbf{x} \rangle = \Re\{\mathbf{y}^H \mathbf{x}\}$.⁶ We assume the following:

- (i) $\mathbf{J}(t, \mathbf{x})$ is full-rank.
- (ii) $H(t, \mathbf{x})$ is uniformly strictly convex, i.e., for some $a > 0$, it holds that

$$D^2H(t, \mathbf{x}) - a\mathbf{I}_n \succeq 0, \text{ for all } t \in \mathbb{R}, \quad (7)$$

and $H(t, \mathbf{x}) = 0 \Leftrightarrow \mathbf{x} = \mathbf{0}_n$.

For the main result on contraction, we consider a ‘‘closed’’ pH system that is without input or output, which is a term coined by J. C. Willems [24]. In the port-Hamiltonian model of a network system [25], each edge is modeled as an ‘‘open’’ pH system, and the input to every edge is mapped from every output by the network constraints:

$$\text{col}(\mathbf{u}_i) = \mathbf{W} \text{col}(\mathbf{y}_i)$$

for some skew-Hermitian network matrix \mathbf{W} . The connected system is written as

$$\dot{\mathbf{x}} = (\mathbf{J}(t, \mathbf{x}) - \mathbf{R})\nabla H(t, \mathbf{x}) \quad (8)$$

where

$$\mathbf{x} = \text{col}(\mathbf{x}_i), H(t, \mathbf{x}) = \sum_i H_i(t, \mathbf{x}_i), \mathbf{R} = \text{diag}(\mathbf{R}_i),$$

$$\mathbf{J}(t, \mathbf{x}) = \text{diag}(\mathbf{J}_i(t, \mathbf{x}_i)) + \text{diag}(\mathbf{G}_i)\mathbf{W} \text{diag}(\mathbf{G}_i^H).$$

The closed pH system (8) has an inherent energy balance relation:

$$\begin{aligned} \dot{H}(t, \mathbf{x}) &= \frac{\partial}{\partial t} H(t, \mathbf{x}) + \Re\{\nabla H(t, \mathbf{x})^H (\mathbf{J}(t, \mathbf{x}) - \mathbf{R})\nabla H(t, \mathbf{x})\} \\ &= \frac{\partial}{\partial t} H(t, \mathbf{x}) - \nabla H(t, \mathbf{x})^H \mathbf{R} \nabla H(t, \mathbf{x}), \end{aligned} \quad (9)$$

where $\mathbf{J}(t, \mathbf{x})$ is energy-preserving because it is skew-adjoint with respect to the assumed inner product.

⁶The subscript for the complex gradient in $\nabla_{\mathbf{x}}H(t, \mathbf{x})$ is omitted in the sequel.

To the best of our knowledge, there exist only two groups of papers dedicated to the contraction of pH systems. In [26], which extends [27], two LMI and one BMI condition are proposed for contractive pH systems. The conditions require lower and upper bounds on the Hessian $D^2H(t, \mathbf{x})$, and in [26, Prop. 3], the interconnection matrix is required to be bounded relative to the damping matrix, similar to the contraction condition for a general NLTV system. In [28], the partial contraction is used to decouple the state-dependence of $\mathbf{A}(\mathbf{x}) = \mathbf{J}(\mathbf{x}) - \mathbf{R}(\mathbf{x})$ from the dynamics, which results in a nonlinear matrix inequality contraction condition; it relies critically on the assumption that the Taylor expansion of the matrix-valued function $\mathbf{A}(\mathbf{x})$ has no first-order term. Both of the two group of results impose upper bound on $D^2H(t, \mathbf{x})$, and constraints on the interconnection (skew-adjoint) $\mathbf{J}(t, \mathbf{x})$ of the dynamics. The main results in Proposition 1 to 4 are free of these constraints; the only additional assumption is for the damping matrix \mathbf{R} to be a constant. This assumption is satisfied at least by the electromagnetic power system model, as the main application in this paper.

III. HORIZONTAL CONTRACTION OF PH SYSTEM

The goal is to introduce a special quotient space associated with the pH system (6) (the canonical quotient space) and to show that the system is contractive with respect to the quotient distance (horizontal contraction). It is then shown that a direct consequence of this property is that the Hamiltonian of the pH system is convergent.

A. The Canonical Quotient Space

A quotient space is a partition of the original space \mathbb{C}^n into subsets called equivalence classes. Every point in the same equivalence class is equivalent; that is distance between them is set to zero. The distance between equivalence classes is defined in terms of a Finsler-like distance. Before we give the definition for this distance, we first define the canonical quotient space of the pH system.

For the pH system (8), at every time instance t , let us consider the quotient space where every equivalence class is an integral curve of the vector field with parameter t :

$$F_t : \mathbf{x} \mapsto \mathbf{J}(t, \mathbf{x}) \nabla H(t, \mathbf{x}). \quad (10)$$

The equivalence class of every $\mathbf{x}_0 \in \mathbb{C}^n$ at time t is

$$[\mathbf{x}_0]_t = \{\Phi_t(\tau, \mathbf{x}_0) \mid \tau \in \mathbb{R}\} \quad (11)$$

where $\Phi_t(\tau, \mathbf{x}_0)$ is the integral curve of (10) from the initial condition \mathbf{x}_0 , i.e.,

$$\begin{aligned} \frac{d}{d\tau} \Phi_t(\tau, \mathbf{x}_0) &= F_t(\Phi_t(\tau, \mathbf{x}_0)) \\ &= \mathbf{J}(t, \Phi_t(\tau, \mathbf{x}_0)) \nabla H(t, \Phi_t(\tau, \mathbf{x}_0)) \end{aligned}$$

Equivalently, the integral curve $\Phi_t(\tau, \mathbf{x}_0)$ is conceptually the solution of the following system with parameter t :

$$\frac{d}{d\tau} \mathbf{x}(\tau) = \mathbf{J}(t, \mathbf{x}(\tau)) \nabla H(t, \mathbf{x}(\tau)) \quad (12)$$

where τ is the independent variable. Since $\mathbf{J}(t, \mathbf{x})$ is skew-Hermitian, we obtain that the value of $H(t, \mathbf{x})$ is constant at

every $\mathbf{x} = \Phi_t(\tau, \mathbf{x}_0)$ for $\tau \in \mathbb{R}$. This is because (12) entails the energy balance $\frac{d}{d\tau} H(t, \mathbf{x}(\tau)) = 0$ where t is a parameter. Hence, at every time instance t , the equivalence class $[\mathbf{x}_0]_t$ belongs to the level set of $H(t, \mathbf{x})$ for \mathbf{x}_0 ; that is,

$$[\mathbf{x}_0]_t \subset \{\mathbf{x} \in \mathbb{C}^n \mid H(t, \mathbf{x}) = H(t, \mathbf{x}_0)\}. \quad (13)$$

Given the definition of the (time-dependent) equivalence classes (11), we can define a (time-dependent) distance measure for any two points $\mathbf{x}_1, \mathbf{x}_2 \in \mathbb{C}^n$. We choose to work with the inner product,

$$\langle \mathbf{y}, \mathbf{x} \rangle = \Re\{\mathbf{y}^H \mathbf{R}^{-1} \mathbf{x}\}. \quad (14)$$

The definitions of norm and orthogonal subspaces for \mathbb{C}^n are consistent with (14). However, with a slight violation of this convention, the definition of the complex gradient $\nabla H(t, \mathbf{x})$ in the pH system (6) is not adapted to (14). This inconsistency is unimportant because the subsequent contraction analysis concerns the derivative of the RHS of (6), i.e., second derivatives of $H(t, \mathbf{x})$. It is chosen to simplify notation.

At every time instance t , the distance measure according to equivalence classes (quotient distance) is defined as follows. By the definition in (10), $\{\mathbf{J}(t, \mathbf{x}) \nabla H(t, \mathbf{x})\}^\perp$ is the tangent subspace perpendicular to the boundary of the equivalence class at \mathbf{x} . For $\mathbf{x} \neq 0_n$, define the local projection operator that projects tangent vectors onto this subspace as

$$\mathcal{P}(t, \mathbf{x}) \delta = \delta - \frac{\langle \mathbf{J}(t, \mathbf{x}) \nabla H(t, \mathbf{x}), \delta \rangle}{\|\mathbf{J}(t, \mathbf{x}) \nabla H(t, \mathbf{x})\| \|\delta\|} \mathbf{J}(t, \mathbf{x}) \nabla H(t, \mathbf{x}), \quad (15)$$

where $\delta \in \mathbb{C}^n \neq 0_n$ is the tangent vector of a curve segment to be defined. It is well-defined because the denominator in (15) is nonzero by the two assumptions near (7). Then, the quotient distance between two points $\mathbf{x}_1, \mathbf{x}_2 \in \mathbb{C}^n$ is defined as the integral of the projected infinitesimal curve segment in (15) along a minimizing curve from \mathbf{x}_1 to \mathbf{x}_2 . To be precise, consider a piecewise smooth curve $\gamma : [0, 1] \rightarrow \mathbb{C}^n$ such that $\gamma(0) = \mathbf{x}_1$, $\gamma(1) = \mathbf{x}_2$, and $\frac{\partial \gamma}{\partial s}(s) \neq 0$. Denote the set of all such curves as $\Gamma(\mathbf{x}_1, \mathbf{x}_2)$. The quotient distance is defined as

$$\text{dist}(t, \mathbf{x}_1, \mathbf{x}_2) = \inf_{\gamma \in \Gamma(\mathbf{x}_1, \mathbf{x}_2)} \int_0^1 \left\| \mathcal{P}(t, \gamma(s)) \frac{\partial \gamma}{\partial s}(s) \right\| ds. \quad (16)$$

The existence of a minimizing curve in (16) is guaranteed by the Gauss lemma [29, Ch. 6]. We list the following properties of the quotient distance (16):

- (i) $\text{dist}(t, \mathbf{x}, \mathbf{y}) = \text{dist}(t, \mathbf{y}, \mathbf{x})$.
- (ii) $\text{dist}(t, \mathbf{y}, \mathbf{x}) \leq \text{dist}(t, \mathbf{y}, \mathbf{z}) + \text{dist}(t, \mathbf{z}, \mathbf{x})$.
- (iii) $\text{dist}(t, \mathbf{y}, \mathbf{x}) = 0$ if $[\mathbf{y}]_t = [\mathbf{x}]_t$ and $\text{dist}(t, \mathbf{y}, \mathbf{x}) \geq 0$ otherwise.
- (iv) If $H(t, \mathbf{y}) \neq H(t, \mathbf{x})$, then $\text{dist}(t, \mathbf{y}, \mathbf{x}) > 0$.

The proof is given in the Appendix.

Remark 1: The projection $\mathcal{P}(t, \mathbf{x})$ defines a local $(n-1)$ -dimensional tangent subspace. Contraction in a tangent subspace (or a horizontal distribution) is referred to as horizontal contraction in Section III-A of [30] where the motivation is to not enforce contraction in the symmetry directions. Note, however, that, for the quotient space defined in (10) and (11), we do not assume that the dynamics of the system preserve the equivalence classes, which is a scenario called a quotient system in Section III-B of [30].

B. Horizontal Contraction in the Quotient Space

The main contraction results are stated without proofs in this subsection. Their proofs are provided in the Appendix.

Definition 1: Let $\Phi(t, t_0, \mathbf{x}_0)$ be the solution of the pH system (6) from the initial condition (t_0, \mathbf{x}_0) . The pH system (6) is said to be *horizontally contracting in the canonical quotient space* (HC for short) if, for some $c > 0$ (the contraction rate), it holds that, for every $\mathbf{x}_1, \mathbf{x}_2 \in \mathbb{C}^n$ and $t_0 \in \mathbb{R}$,

$$\text{dist}(t, \Phi(t, t_0, \mathbf{x}_1), \Phi(t, t_0, \mathbf{x}_2)) \leq e^{-c(t-t_0)} \text{dist}(t_0, \mathbf{x}_1, \mathbf{x}_2). \quad (17)$$

The pH system is said to be weakly HC if (17) holds with $c = 0$. \diamond

The following two results concern the intrinsic contraction properties of the pH system.

Proposition 1 (Horizontal Contraction with $\mathbf{R} \succ 0$): The closed pH system (8) that has a uniformly strictly convex Hamiltonian, i.e., condition (7), is HC with the contraction rate,

$$c = \min_{t \in \mathbb{R}} \lambda_{\min}(D^2 H(t, \mathbf{x})) \lambda_{\min}(\mathbf{R}),$$

where $\lambda_{\min}(\mathbf{A})$ is the smallest eigenvalue of the Hermitian matrix \mathbf{A} . \diamond

Proposition 2 (Weak Horizontal Contraction with $\mathbf{R} = \mathbf{0}$): The closed pH system (8) that has a uniformly strictly convex Hamiltonian, i.e., condition (7), and zero dissipation, i.e., $\mathbf{R} = \mathbf{0}$, is weakly HC. \diamond

Remark 2: The classical Hamiltonian dynamics with a time-varying strictly convex Hamiltonian is covered by Proposition 2 with the interconnection matrix $\mathbf{J} = [\mathbf{0}, \mathbf{I}; -\mathbf{I}, \mathbf{0}]$. \diamond

The following two results concern the implications of HC on the behavior of the solutions.

Proposition 3 (Converging Hamiltonian Difference): Consider the closed and HC pH system (8). Let $\bar{\mathbf{x}}(t)$ be a particular solution. Then, the Hamiltonian value converges to $H(t, \bar{\mathbf{x}}(t))$ from every initial value, i.e., from every initial condition (t_0, \mathbf{x}_0) , $\lim_{t \rightarrow \infty} H(t, \Phi(t, t_0, \mathbf{x}_0)) - H(t, \bar{\mathbf{x}}(t)) = 0$. \diamond

Remark 3: By definition, every equivalence class of the canonical quotient space is 1D; meanwhile, every level set of the Hamiltonian $H(t, \mathbf{x})$ for a fixed t has dimension $2n - 1$ (since \mathbb{C}^n has the same dimension as \mathbb{R}^{2n}). For $n = 1$ (every level set is 1D and coincides with an equivalence class), then HC implies difference in the Hamiltonian values converges at the exponential rate e^{-ct} . For $n > 1$ (every level set has dimension higher than one), then exponential contraction of the difference in the Hamiltonian values is not guaranteed. \diamond

The following is the main condition for the convergence of the Hamiltonian, i.e., convergence to a single constant value.

Proposition 4 (Hamiltonian Convergence Principle): Consider the closed and HC pH system (8). Assume that the set in which the Hamiltonian has zero derivative, i.e.,

$$E_t = \left\{ \mathbf{x} \in \mathbb{C}^n \mid \frac{\partial}{\partial t} H(t, \mathbf{x}) - \nabla H(t, \mathbf{x})^H \mathbf{R} \nabla H(t, \mathbf{x}) = 0 \right\},$$

is time-independent. Then, the Hamiltonian value converges from every initial value, i.e., from every initial condition

(t_0, \mathbf{x}_0) , $\lim_{t \rightarrow \infty} H(t, \Phi(t, t_0, \mathbf{x}_0)) = \bar{H}$ for some constant $\bar{H} \geq 0$. \diamond

The set E_t in Proposition 4 is usually found to be time-independent because the system can be alternatively written as a time-invariant system. In most applications, including the power system model to be introduced, the time dependence of the Hamiltonian represents a power source; that is,

$$\eta(\mathbf{x}) = \frac{\partial}{\partial t} H(t, \mathbf{x})$$

represents the the input power.⁷ It is a mathematical technique to represent state-dependent power input/output without introducing negative eigenvalues into the damping matrix \mathbf{R} . If a time-invariant form of the system exists, then the set E_t , which represents the states where the stored energy is steady, can be alternatively defined by a time-independent condition, and is hence a time-independent set.

When the system has a power input, the limit set or steady state usually cannot be described by an equilibrium point (for example the van der Pol equation [23]). In this case, the limit set is the result of a balance between the power input and dissipation. For studying these systems, Proposition 4 asserts that, if the power input can be mathematically expressed as a time-dependence part of the Hamiltonian, then the limit set is contained in a level set of the original time-independent Hamiltonian. On the possible types of limit sets, if the dimension of the system is 3 and the dimension of the level set is 2, then by the Poincare-Bendixson theorem [23], the limit set must be a limit cycle. If the dimension of the system greater than 3, more complicated limit sets may exist (a chaos).

IV. STABILITY OF THE ELECTROMAGNETIC POWER SYSTEM MODEL

The electromagnetic model or the fundamental model is different from the electromechanical model in that the fundamental inductor and capacitor equations are included, rather than simplified into linear impedance equations. The impedance equations are based on the assumption of a steady state of a synchronized frequency throughout the system, omitting all other types of limit cycles and necessitating separate harmonic power flow studies [33]. The difficulty in studying the electromagnetic model is twofold. First, the dimension of the system including the inductor fluxes and the capacitor charges is much higher. Second, the inductor and capacitor dynamics are much faster than the mechanical dynamics of the synchronous generator (SG). Attempts on the hard problem of extending the electromechanical stability conditions to the electromagnetic model lead to overly conservative conditions [34], [35].

We consider in this section the stability of the electromagnetic power system model. As the main application of Proposition 4, we show that the convergence of the Hamiltonian is sufficient for stability assuming that a desirable limit cycle steady state exists. To this end, we first introduce the physical model of the SG, followed by its formulation into a time-varying pH system that is covered by Proposition 4. Then,

⁷We refer the reader to [31], [32] for some perspectives on port-Hamiltonian system with power input.

the model of a power system with two SG is provided as an example. Lastly, the stability of this model is proved.

A. Physical Model in $\alpha\beta$ -Coordinates

Assume the motor sign convention, i.e., positive stator current goes into the machine. The mechanical dynamics is given by the swing equation:

$$J\dot{\omega} = -F\omega - T_e + T_m \quad (18)$$

$$\dot{\theta} = \omega, \quad (19)$$

where ω is the rotor angular frequency, θ is the rotor angle, J is the rotational inertia, F is the viscous damping, and T_e and T_m are respectively the (accelerating) electrical and mechanical torque.⁸

We assume balanced condition such that the 0-phase in the stationary $\alpha\beta 0$ -coordinates is a decoupled DC system whose state is constant zero [38]. Choose the complex variable $I = I^\alpha + jI^\beta$ for the stator current and $V = V^\alpha + jV^\beta$ for the terminal voltage. Let $\psi = MI_F \in \mathbb{R}$ be the constant field flux, i.e., mutual inductance M times the field current I_F . The stator equation is given by

$$L\dot{I} = -\psi(j\omega e^{j\theta}) - RI + V,$$

where R is the stator current, and $-\psi(j\omega e^{j\theta})$ is the internal EMF. To complete the swing equation (18), note that the electrical torque is equal to the power transfer divided by the frequency:

$$T_e = \frac{\Re\{-\psi(j\omega e^{j\theta})I^H\}}{\omega} = \Re\{j\psi e^{-j\theta}I\},$$

Assume that the mechanical source has droop characteristic:

$$T_m = T_0 - F_1\omega,$$

where F_1 is the torque droop ratio, and T_0 is the projected zero-frequency torque. Then we obtain the controlled swing equation,

$$J\dot{\omega} = -F\omega - \Re\{j\psi e^{-j\theta}I\} + T_0,$$

where we absorbed $F \leftarrow F + F_1$.

B. Time-Varying PH Model

Choose the state vector $\mathbf{x} = [\mathbf{x}_1, \theta]^T \in \mathbb{R} \times \mathbb{C} \times \mathbb{T}$ where

$$\mathbf{x}_1 = [x_1, x_2]^T = [J\omega - T_0t, LI]^T. \quad (20)$$

The space \mathbb{T} is the 2π -periodic torus [18] for the angle. The equations for the state vector are given by

$$\frac{d}{dt}(J\omega - T_0t) = -F\omega - \Re\{j\psi\omega e^{-j\theta}I\} \quad (21)$$

$$\frac{d}{dt}(LI) = -j\psi\omega e^{j\theta} - RI + V \quad (22)$$

$$\frac{d}{dt}\theta = \omega. \quad (23)$$

⁸We refer the reader to [15], [36], [37] for perspectives on the difficulty in studying the stability of systems in periodic angle spaces, i.e., the 2π periodic torus space \mathbb{T} in which θ lives.

Define the Hamiltonian as

$$H(t, \mathbf{x}_1) = \frac{1}{2}J^{-1}(x_1 + T_0t)^2 + \frac{1}{2}L^{-1}\|x_2\|^2,$$

which is equal to the inertial energy plus the magnetic energy. The gradient of the Hamiltonian is

$$\nabla H(t, \mathbf{x}_1) = \begin{bmatrix} J^{-1}(x_1 + T_0t) \\ L^{-1}x_2 \end{bmatrix} = \begin{bmatrix} \omega \\ I \end{bmatrix}. \quad (24)$$

Note that the Hamiltonian can be alternatively expressed as

$$H(t, \mathbf{x}_1) = H(\mathbf{s}) = \frac{1}{2}\mathbf{s}^H\mathbf{Q}^{-1}\mathbf{s}$$

with the co-state $\mathbf{s} = \nabla H(t, \mathbf{x})$ and $\mathbf{Q} = \text{diag}(J^{-1}, L^{-1})$. We can find the real Hessian of the Hamiltonian as⁹

$$D^2H(t, \mathbf{x}_1) = \begin{bmatrix} J^{-1} & 0 \\ 0 & L^{-1}\mathbf{I} \end{bmatrix} \quad (25)$$

for the equivalent real state vector, $\mathcal{U}\mathbf{x}_1 = [J\omega - T_0t, LI^\alpha, LI^\beta]^T$. Since $J, L > 0$, the Hamiltonian is uniformly strictly convex. Based on (20) and (24), the pH model for \mathbf{x}_1 is obtained as

$$\Sigma_{sg} : \begin{cases} \dot{\mathbf{x}}_1 = \mathcal{W}[(\mathbf{J}(\theta) - \mathbf{R})\nabla H(t, \mathbf{x}_1) + \mathbf{G}\mathbf{u}] \\ \mathbf{y} = \mathbf{G}^H\nabla H(t, \mathbf{x}_1) \end{cases}, \quad (26)$$

where $\mathbf{u} = V$, $\mathbf{y} = I$,

$$\mathcal{W} = \begin{bmatrix} \Re & 0 \\ 0 & 1 \end{bmatrix}, \quad \mathbf{G} = \begin{bmatrix} 0 \\ 1 \end{bmatrix},$$

and

$$\mathbf{J}(\theta) = \begin{bmatrix} 0 & -j\psi e^{-j\theta} \\ -j\psi e^{j\theta} & 0 \end{bmatrix}, \quad \mathbf{R} = \begin{bmatrix} F & 0 \\ 0 & R \end{bmatrix}.$$

For the dynamics (26), the inner product assumed is

$$\langle \mathbf{y}, \mathbf{x} \rangle = \Re\{(\mathcal{W}\mathbf{y})^H(\mathcal{W}\mathbf{x})\}.$$

Note that the SG system (21)–(23) is not exactly an open pH system (6); the pH system for the SG in (26) does include the last equation (23) while the physical Hamiltonian $H(t, \mathbf{x}_1)$ is not dependent on the angle θ . Note, however, that the main propositions in Section III still apply to this system with the minimal modification as follows. For the quotient distance in (16), the projection of the \mathbf{x}_1 dimensions is defined as in (15), i.e.,

$$\mathcal{P}(t, \mathbf{x}) \begin{bmatrix} \delta_1 \\ 0 \end{bmatrix} = \begin{bmatrix} \delta_1 - \frac{\langle \mathbf{J}(\theta)\nabla H(t, \mathbf{x}_1), \delta_1 \rangle}{\|\mathbf{J}(\theta)\nabla H(t, \mathbf{x}_1)\| \|\delta_1\|} \mathbf{J}(\theta)\nabla H(t, \mathbf{x}_1) \\ 0 \end{bmatrix}$$

for $\delta_1 \in T_{\mathbf{x}_1}(\mathbb{R} \times \mathbb{C}) = \mathbb{R} \times \mathbb{C}$, and the projection of the θ dimension is set to 0, i.e.,

$$\mathcal{P}(t, \mathbf{x}) \begin{bmatrix} 0 \\ 0 \\ \delta\theta \end{bmatrix} = \begin{bmatrix} 0 \\ 0 \\ 0 \end{bmatrix}$$

for $\delta\theta \in T_{\mathbf{x}}\mathbb{T} = \mathbb{R}$. Then, it is easy to checked that the proofs of the main propositions in Section III still work under the respective conditions.

⁹The set of independent variables are $\{\mathbf{x}, t\}$. All partial derivatives are defined with respect to these independent variables.

We can check the condition of Proposition 4 as follows, Note that, from (9), the power input is $\frac{\partial}{\partial t} H(t, \mathbf{x}_1) = T_0 \omega$, and the dissipation is $-\mathbf{s}^H \mathbf{R} \mathbf{s}$. Both are time-independent. Then, by Proposition 4, the Hamiltonian is convergent if we ignore the input. The input is supplied from other subsystems of the power system, which are introduced in the next subsection.

Remark 4: The technique for modeling the SG with constant field current as a pH system can be easily applied to the full-order SG dynamics with one excitation winding and three damper windings [39]. To do this, the DC circuits are modeled as real variables similar to x_1 in the above. We choose to present the simpler SG model in this paper to show the idea more clearly. \diamond

C. Two-Machine System with Constant Impedance Loads

As an example, consider a two-machine system with constant impedance loads. With the pH modeling technique introduced in [25], the system is seen as a directed graph where each edge is either a SG, a shunt capacitor, or an R-L line. The sign convention for the edge voltage and current follows the direction of the edge; that is positive edge voltage and current consumes real power. See Fig. 1 for the graph topology of the two-machine system considered.

The two SG systems are denoted as Σ_{sg_i} , $i \in \{1, 2\}$. The transmission lines are modeled by the lumped-parameter Π -model [40]. The equations for the shunt capacitor edge is, for $i \in \{3, 4, 5\}$,

$$\Sigma_{sh_i} : \begin{cases} \frac{d}{dt}(C_i V_i) = -Y_i \nabla H_i(C_i V_i) + I_i \\ V_i = \nabla H_i(C_i V_i) \end{cases}, \quad (27)$$

where V_i and I_i are respectively the edge voltage and current, $H_i(\mathbf{x}_i) = \frac{1}{2} C_i^{-1} \|\mathbf{x}_i\|^2$ with $\mathbf{x}_i = C_i V_i$, Y_i with $\Re\{Y_i\} > 0$ is the admittance of the constant impedance load. The equations for the line edges are, for $i \in \{6, 7\}$,

$$\Sigma_{ln_i} : \begin{cases} \frac{d}{dt}(L_i I_i) = -R_i \nabla H_i(L_i I_i) + V_i \\ I_i = \nabla H_i(L_i I_i) \end{cases}, \quad (28)$$

where V_i and I_i are respectively the edge voltage and current; $H_i(\mathbf{x}_i) = \frac{1}{2} L_i^{-1} \|\mathbf{x}_i\|^2$ with $\mathbf{x}_i = L_i I_i$; R_i is the series line resistance.

Based on the inputs and outputs,

$$\mathbf{u} = [V_1, V_2, I_3, I_4, I_5, V_6, V_7]^T, \\ \mathbf{y} = [I_1, I_2, V_3, V_4, V_5, I_6, I_7]^T.$$

and KCL and KVL, the network matrix which relates the inputs and outputs of the edges, is found as

$$\mathbf{W} = \begin{bmatrix} 0 & 0 & 1 & 0 & 0 & 0 & 0 \\ 0 & 0 & 0 & 1 & 0 & 0 & 0 \\ -1 & 0 & 0 & 0 & 0 & -1 & 0 \\ 0 & -1 & 0 & 0 & 0 & 0 & -1 \\ 0 & 0 & 0 & 0 & 0 & 1 & 1 \\ 0 & 0 & 1 & 0 & -1 & 0 & 0 \\ 0 & 0 & 0 & 1 & -1 & 0 & 0 \end{bmatrix}.$$

We verify that that \mathbf{W} is skew-symmetric. Hence, recalling (8), the two-machine system connected through \mathbf{W} is a pH

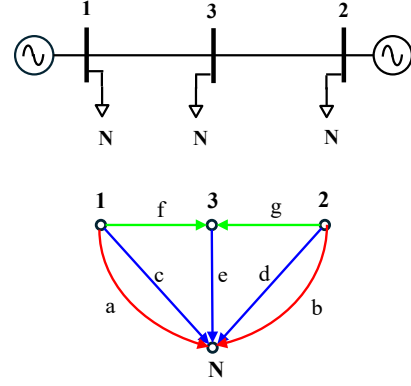


Fig. 1. Single-line diagram of the two-machine system and the underlying graph topology (SG: red, shunt capacitor: blue, R-L line: green)

system with $\mathbf{R} \succ 0$ and $D^2 H(t, \mathbf{x}) - a \mathbf{I}_n \succeq 0$. Note that the skew-symmetry of the network matrix results from KVL and KCL, and so it holds regardless of the topology of the power system [41].

D. Stability of the Two-Machine System

To prove the stability of the two-machine system, we need the following result on the uniqueness of the limit cycle of an RLC circuit with sinusoidal forcing.

Lemma 1: Consider an RLC circuit with sinusoidal forcing. With the edge dynamics given by (27) and (28), the equations can be written in the form,

$$\dot{\mathbf{x}} = (\mathbf{J} - \mathbf{R}) \nabla H(\mathbf{x}) + \mathbf{g} u$$

with $u = e^{j\omega_0 t}$ and $H(\mathbf{x}) = \frac{1}{2} \mathbf{x}^H \mathbf{Q} \mathbf{x}$ for diagonal \mathbf{Q} and \mathbf{R} . Assume the system has a limit cycle $\bar{\mathbf{x}}(t) = e^{j\omega_0 \tau} \bar{\mathbf{x}}(0)$. Then the orbit of the limit cycle is the only possible limit set. \diamond

The proof is given in the Appendix.

Proposition 5: Assume the two-machine system has a limit cycle solution $\bar{\mathbf{x}}(t)$ of a synchronized frequency $\bar{\omega} \in \mathbb{R}$ such that the complex variables change as $x_i(t) = e^{j\bar{\omega} t} x_i(0)$. Then every solution of the system converges to the limit cycle solution as $t \rightarrow \infty$. \diamond

The proof is given in the Appendix.

Since the proof for the two-machine system does not rely on the graph topology, the same stability result can be generalized to multi-machine systems with constant impedance loads. For the sake of the analysis, the only difference is the dimensionality of the network matrix. In general, one can consider distributed-parameter model of the transmission lines where the number of edges approaches infinity [40].

Proposition 6: Assume that a multi-machine system consisting of SG, shunt capacitor, and R-L line edges, has a limit cycle solution of a synchronized frequency. Then every solution of the system converges to the limit cycle solution as $t \rightarrow \infty$. \diamond

The proof is similar to the proof of Proposition 5 and is omitted.

Remark 5: By Proposition 1, the convergence rate of the Hamiltonian is proportional to $\lambda_{\min}(D^2 H(t, \mathbf{x})) \lambda_{\min}(\mathbf{R})$. Assuming that the mechanical energy storage is dominant in

TABLE I
PARAMETERS OF THE TWO-MACHINE TEST SYSTEM

Description	Parameter
SG mechanical	$J = 2.846 \times 10^4 \text{ kg} \cdot \text{m}^2$, $F = 85.5601 \text{ N} \cdot \text{m} \cdot \text{s}$, $p = 4$, $T_0 = 1 \times 10^4 \text{ N} \cdot \text{m}$
SG electrical	$R_s = 1.542 \text{ m}\Omega$, $L_s = 6.341 \text{ mH}$, $\psi = 39.7877 \text{ V} \cdot \text{s}$
Shunt capacitor	$C_{sh,3} = 50 \text{ mF}$, $C_{sh,4} = 100 \text{ mF}$, $C_{sh,5} = 50 \text{ mF}$
Load	$R_{ld,3} = 1 \text{ k}\Omega$, $L_{ld,3} = 10 \text{ H}$ $R_{ld,4} = 4 \Omega$, $L_{ld,4} = 1 \text{ H}$ $R_{ld,5} = 1 \text{ k}\Omega$, $L_{ld,5} = 10 \text{ H}$
R-L line	$R_{ln,6} = 3 \Omega$, $L_{ln,6} = 1.061 \text{ H}$, $R_{ln,7} = 3 \Omega$, $L_{ln,7} = 1.061 \text{ H}$

$H(t, \mathbf{x})$ and the electrical energy dissipation is dominant in \mathbf{R} , we obtain that the convergence rate of the power system Hamiltonian is estimated as $\min\{\Re Y_i\} / \max\{J_i\}$. \diamond

V. NUMERICAL EXAMPLES

In Proposition 5, we proved that a limit cycle of the power system with constant impedance loads, is globally convergent if it exists. Note that stability in power system traditionally refers the steady-state behavior of the system; this includes

1. convergence of all the SG frequencies to a single constant synchronized frequency,
2. no low-frequency oscillations, i.e., the envelope of every three-phase AC signal is a straight horizontal line,
3. no harmonics, i.e., every AC signal has a single Fourier component at the synchronized frequency from (i).

We will show that these steady-state instability conditions do not contradict with the global convergence result proved in Proposition 5 because the traditional stability concerns the regularity of the steady state as opposed to its convergence property. Here we should adopt a geometric approach to the system by considering its set of solutions that has ran for all finite time. The steady state, be it a *synchronized limit cycle* or an *imperfect (negation of 1–3) limit cycle*, is the target set whose Hamiltonian value is convergent, and, in the case of a synchronized limit cycle, the orbit is convergent as well. In fact, we will show that the instability of the steady-state in traditional power engineering correspond to the nonexistence of a synchronized limit cycle, due to the conflict between the power flow constraint from the RLC network and the power injection constraint from the SGs.

The two machine system in Fig. 1 is chosen. A electromagnetic model is build in Simulink Specialized Power System in SI units. The PMSM model is used to model a SG with constant field current. The parameters of the SG are obtained from Example 4.1 from [39], which are given in Table I as well as all the other parameters.

A. Global Convergence in the Regular Case

In the first case, we set the parameters of the system such that there is reflection symmetry between the left and right half of the topology. This ensures that a synchronized limit cycle

exists so that we can test convergence alone. More generally, a symmetric radial network is similar to a single SG system, and so a synchronized limit cycle exists [42]. We test the convergence property of the system by starting from a random initial condition generated by $100 \cdot \text{rand}(26)$ for 26 real state variables. We can see from Fig. 2d that immediately after the initial condition there is a large overshoot in the Hamiltonian caused by the RLC network quickly returning to an almost quasi steady state. Between 0 s and 485 s, the waveform of the voltage is not regular at all as it exhibits low-frequency oscillation. During this time, the voltage waveform appears constant except for the increasing widths of the distinct wave packets, while the rotor frequencies continue to approach each other. Between 485 s and 700 s, the rotor frequencies are locked to each other, and the low-frequency oscillation is dying. At around 700 s, the system returns to the synchronized limit cycle with a single-frequency waveform. We tested 50 other initial conditions from $1000 \cdot \text{rand}(26)$ to verify that the system returns to the same synchronized limit cycle. We tested multiplying the damping matrix by a factor and observe that the transient time reduces by the same factor. We also tested multiplying the SG inertia by a factor of the nominal value and observed that the qualitative behavior of the system remains the same except that the transient time is extended with higher inertias and shortened with lower inertias.

Note that the initial conditions tested here are much farther from the synchronized limit cycle compared to those considered in traditional power system stability studies—the initial condition is far outside the region of convergence predicted by the direct method. Moreover, in traditional power engineering, the excitation control is considered to have a the biggest effect on (steady-state) stability, whereas, here, the field current is kept constant. The transient condition tested here corresponds to uncontrolled black starts or protection device malfunctioning in faults where the rotor angle stability [4] is lost. The test result shows that the traditional stability concepts such as critical clearing time, and the negative effect of low inertia on stability, do not hold at least for this test system. We suspect the reason for these traditional concepts is that it takes two distinct stages for the state to converge. From Fig. 2, there is almost no sign that the low-frequency oscillation is dying before 485 s while the rotor frequencies are approaching each other. This behavior is qualitatively different from the more familiar linear dynamics where convergence is exponential in every state variable.

B. Loss of Synchronized Limit Cycle Steady State

There are several ways that a synchronized limit cycle cannot be reached asymptotically. In the first case, we increased the torque input of SG 2 from $1 \times 10^4 \text{ N} \cdot \text{m}$ to $1.5 \times 10^4 \text{ N} \cdot \text{m}$ so that right side of the two-machine system will inject 1.5 times the power than the left side if the two rotor frequencies are to converge to the same value. As we can see from Fig. 3, the frequencies of the two machines converge to different values. The frequency of SG 2 is approximately 1.5 times the frequency of SG 1, possibly due to the additional torque input. The steady state shown in Fig. 3b shows that the steady-state limit cycle

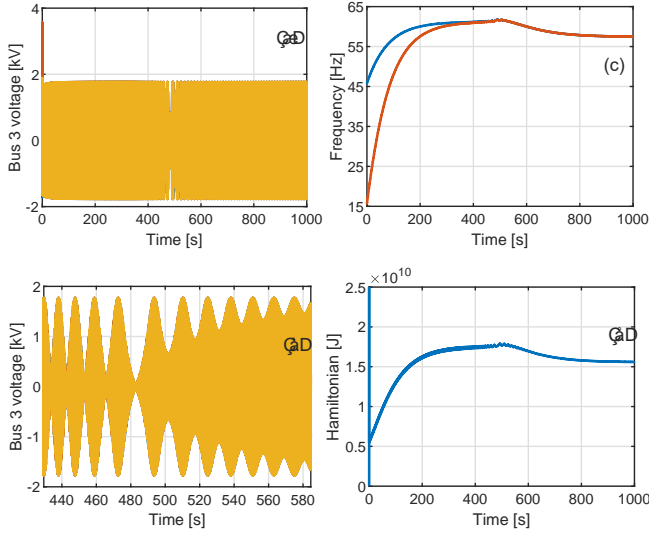


Fig. 2. Case where there exists a synchronized limit cycle

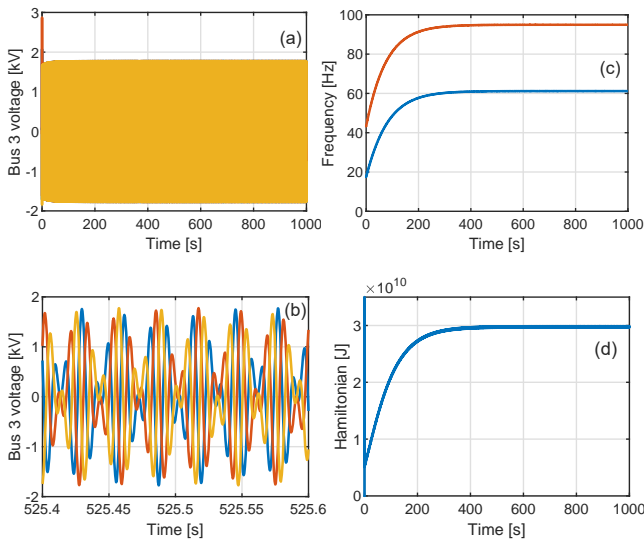


Fig. 3. Case where there only exists an imperfect limit cycle with low-frequency oscillation (existence of two steady-state frequencies) due to the large difference between the input torques of the two SGs

exhibits low-frequency oscillation which forms distinct wave packets. This otherwise undamped low-frequency oscillation is damped in practice by excitation control which modulates the excitation voltage based on measurement of the terminal voltage [39].

In the second case, we multiplied the constant field flux of both SGs by 2.5 times. We can see from Fig. 4 that the voltage and the frequency both collapse to close to zero after a transient period. This is because the high field flux results in high EMF, which results in high real power consumption from the constant impedance loads, compared to the relatively low torque input. Note that, even in this case, the final steady state is not exactly zero, but is an equilibrium point that is very close to zero—the zero state is not stable whenever the

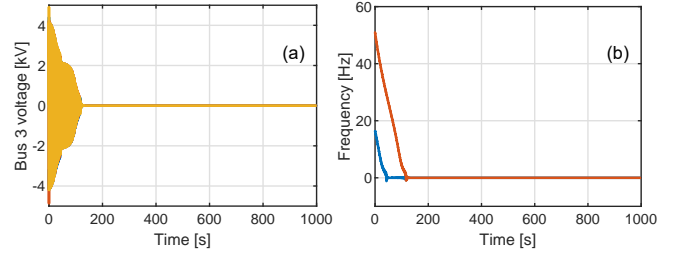


Fig. 4. Case where the system collapses to close to zero due to the field fluxes of the SGs being too high

input torque is nonzero.

In the third case, we observed during our test that, under certain parameter choices, the system goes into a bounded chaotic state rather than a limit cycle.

C. Discussion

It is shown that global stability, i.e., convergence of every solution to a synchronized limit cycle, holds for multi-machine power system dynamics if the synchronized limit cycle exists. The convergence rate is observed to be proportional to $1/\max\{J_i\}$ and $\min\{\Re\{Y_i\}\}$. It is justified both theoretically and experimentally that the remaining question to ask about power system dynamics is whether the synchronized limit cycle exists, because it is stable if it exists. This explains why the focus on phasor analysis in traditional power engineering has proved successful thus far, despite the highly nonlinear dynamics. The revealed stability property of the traditional SG power system is insightful for the control of inverter-based resources (IBR). Although the SG dynamics implies globally stability, there is still room to design IBR control schemes to improve transient smoothness and power sharing as the future power system is seeing more frequent reconfigurations. See our work toward this direction in [41].

From the test results, we can see that the biggest challenge in operating AC power system versus DC power system is not in stability but the potentially complicated steady-state behavior. The steady state behaviors of AC system include undesirable oscillations and chaos. These important features of the steady state cannot be represented in the traditional phasor analysis, and not fully by harmonic power flow studies. For future research, more research effort is needed toward the precise steady state behaviors of AC power systems to obtain conditions on the existence of synchronized limit cycles and the corresponding steady state control schemes. A notable recent work toward this direction is [43].

VI. CONCLUSION

This paper presents a theoretical analysis of the novel CQS property of the time-varying pH system and applied it to the stability analysis of the electromechanical model of the power system. It is found that, if the system has a synchronized limit cycle, then its orbit is globally convergent. In the case study of a two-machine system, we verified this stability result and identified that several instability concepts in traditional power

engineering are related to the nonexistence of the synchronized limit cycle. The contributions of this paper is threefold. Firstly, it provides a rigorous analysis of power system stability, which unifies the common instability phenomena in power systems. It is identified that the main challenge in the operation of future AC power systems with high power electronics penetration is the existence of a synchronized limit cycle. Secondly, the converging Hamiltonian principle provides an elegant way to characterize the stability of systems with power sources, exhibiting limit cycle behavior. Thirdly, the horizontal contraction property of time-varying pH system is applicable to the stabilization of periodic motions in other areas such as robotics and multi-agent systems.

APPENDIX

A. Proof of Properties (i)–(iv) of the Quotient Distance (16)

(i) Denote $V(\mathbf{x}, \delta) = \|\mathcal{P}(t, \mathbf{x})\delta\|$. Since $V(\mathbf{x}, -\delta) = V(\mathbf{x}, \delta)$, the pseudo-metric (16) is symmetric, which implies (i).

(ii) It is implied from the principle of dynamic programming.

(iii) The quotient distance (16) being nonnegative is obvious. If $[\mathbf{x}_1]_t = [\mathbf{x}_2]_t$, then, by the definition (10), there is an integral curve of (10) that joins \mathbf{x}_1 and \mathbf{x}_2 . The tangent vectors of this integral curve are orthogonal to span of the projection $\mathcal{P}(\mathbf{x}, \delta)$ by definition. Therefore, this curve causes the integral in the RHS of (16) to evaluate to zero, which, combined with nonnegativity, implies $\text{dist}(\mathbf{x}_1, \mathbf{x}_2) = 0$.

(iv) From (13), each equivalence class is contained in a level set of $H(t, \mathbf{x})$. Since tangent vector of the equivalence class is $\text{span}(\mathcal{P}(t, \mathbf{x}))^\perp$, $\nabla H(t, \mathbf{x}) \in \text{span}(\mathcal{P}(t, \mathbf{x}))$. Then, for each \mathbf{x}, \mathbf{y} with $H(t, \mathbf{x}) \neq H(t, \mathbf{y})$, it holds that $\text{dist}(t, \mathbf{y}, \mathbf{x}) \geq \min \{\|\mathbf{z}_1 - \mathbf{z}_2\| \mid H(t, \mathbf{z}_1) = H(t, \mathbf{x}), H(t, \mathbf{z}_2) = H(t, \mathbf{y})\} > 0$, where we expanded each equivalence relation to entire level set for the first inequality and used that level sets are disjoint and closed for the second inequality. \square

B. Proof of Proposition 1

1. From Grönwall's lemma, to prove (17), it suffices to prove that

$$\begin{aligned} & \frac{d}{dt} \text{dist}(t, \Phi(t, t_0, \mathbf{x}_1), \Phi(t, t_0, \mathbf{x}_2)) \\ & \stackrel{?}{\leq} -c \text{dist}(t, \Phi(t, t_0, \mathbf{x}_1), \Phi(t, t_0, \mathbf{x}_2)). \end{aligned} \quad (29)$$

Using (16), we can express (29) as

$$\begin{aligned} & \frac{d}{dt} \text{dist}(t, \Phi(t, t_0, \mathbf{x}_1), \Phi(t, t_0, \mathbf{x}_2)) \\ & = \frac{d}{dt} \min_{\gamma \in \Gamma(\Phi(t, t_0, \mathbf{x}_1), \Phi(t, t_0, \mathbf{x}_2))} \int_0^1 \left\| \mathcal{P}(t, \gamma(s)) \frac{\partial \gamma}{\partial s}(s) \right\| ds \\ & \leq \frac{d}{dt} \int_0^1 \left\| \mathcal{P}(t, \psi(t, s)) \frac{\partial \psi}{\partial s}(t, s) \right\| ds \end{aligned} \quad (30)$$

$$\begin{aligned} & \stackrel{?}{\leq} -c \int_0^1 \left\| \mathcal{P}(t, \psi(t, s)) \frac{\partial \psi}{\partial s}(t, s) \right\| ds \\ & = -c \text{dist}(t, \Phi(t, t_0, \mathbf{x}_1), \Phi(t, t_0, \mathbf{x}_2)), \end{aligned} \quad (31)$$

where $\psi(t, s)$ is a curve that achieves the minimum at $t = t_0$, and $\psi(t, s) = \Phi(t, t_0, \psi(t, s))$ is the solution of the system

rooted at $\psi(t_0, s) = \psi(t, s)$, $s \in [0, 1]$. The inequality (30) holds because the curve $\psi(t, s)$ is either minimizing or not for $t > t_0$. Note that, to prove the inequality (31), it suffices to prove that the integrand satisfies the inequality uniformly, i.e.,

$$\frac{d}{dt} \left\| \mathcal{P}(t, \psi(t, s)) \frac{\partial \psi}{\partial s}(t, s) \right\| \stackrel{?}{\leq} -c \left\| \mathcal{P}(t, \psi(t, s)) \frac{\partial \psi}{\partial s}(t, s) \right\|. \quad (32)$$

The inequality (32) is equivalent to

$$\begin{aligned} & \frac{1}{2} \frac{d}{dt} \left\langle \mathcal{P}(t, \psi(t, s)) \frac{\partial \psi}{\partial s}(t, s), \mathcal{P}(t, \psi(t, s)) \frac{\partial \psi}{\partial s}(t, s) \right\rangle \\ & \stackrel{?}{\leq} -c \left\langle \mathcal{P}(t, \psi(t, s)) \frac{\partial \psi}{\partial s}(t, s), \mathcal{P}(t, \psi(t, s)) \frac{\partial \psi}{\partial s}(t, s) \right\rangle, \end{aligned} \quad (33)$$

because, for any $m(t) \geq 0$, $\frac{d}{dt} m \leq -cm \Leftrightarrow \frac{1}{2} \frac{d}{dt} m^2 \leq -cm^2$. 2. The LHS of (33) can be manipulated as

$$\begin{aligned} & \frac{1}{2} \frac{d}{dt} \left\langle \mathcal{P}(t, \psi(t, s)) \frac{\partial \psi}{\partial s}(t, s), \mathcal{P}(t, \psi(t, s)) \frac{\partial \psi}{\partial s}(t, s) \right\rangle \\ & = \left\langle \mathcal{P}(t, \psi(t, s)) \frac{\partial \psi}{\partial s}(t, s), \frac{d}{dt} \left[\mathcal{P}(t, \psi(t, s)) \frac{\partial \psi}{\partial s}(t, s) \right] \right\rangle \\ & = \left\langle \mathcal{P}(t, \psi(t, s)) \frac{\partial \psi}{\partial s}(t, s), \mathcal{P}(t, \psi(t, s)) \frac{\partial}{\partial t} \frac{\partial \psi}{\partial s}(t, s) \right\rangle \\ & \quad + \left\langle \mathcal{P}(t, \psi(t, s)) \frac{\partial \psi}{\partial s}(t, s), \frac{d}{dt} \mathcal{P}(t, \psi(t, s)) \frac{\partial \psi}{\partial s}(t, s) \right\rangle \\ & = \left\langle \mathcal{P}(t, \psi(t, s)) \frac{\partial \psi}{\partial s}(t, s), \frac{\partial}{\partial \mathbf{x}} \left[\mathcal{P}(t, \psi(t, s)) \frac{\partial}{\partial t} \psi(t, s) \right] \frac{\partial \psi}{\partial s}(t, s) \right\rangle \\ & \quad - \left\langle \mathcal{P}(t, \psi(t, s)) \frac{\partial \psi}{\partial s}(t, s), \frac{\partial}{\partial \mathbf{x}} \mathcal{P}(t, \psi(t, s)) \frac{\partial \psi}{\partial t}(t, s) \frac{\partial \psi}{\partial s}(t, s) \right\rangle \\ & \quad + \left\langle \mathcal{P}(t, \psi(t, s)) \frac{\partial \psi}{\partial s}(t, s), \frac{d}{dt} \mathcal{P}(t, \psi(t, s)) \frac{\partial \psi}{\partial s}(t, s) \right\rangle \quad (34) \\ & = \left\langle \mathcal{P}(t, \psi(t, s)) \frac{\partial \psi}{\partial s}(t, s), \frac{\partial}{\partial \mathbf{x}} \left[\mathcal{P}(t, \psi(t, s)) \frac{\partial}{\partial t} \psi(t, s) \right] \frac{\partial \psi}{\partial s}(t, s) \right\rangle \\ & \quad + \left\langle \mathcal{P}(t, \psi(t, s)) \frac{\partial \psi}{\partial s}(t, s), \frac{\partial}{\partial t} \mathcal{P}(t, \psi(t, s)) \frac{\partial \psi}{\partial s}(t, s) \right\rangle \quad (35) \\ & = \left\langle \mathcal{P}(t, \psi(t, s)) \frac{\partial \psi}{\partial s}(t, s), \frac{\partial}{\partial \mathbf{x}} [-\mathbf{R} \nabla H(t, \psi(t, s))] \frac{\partial \psi}{\partial s}(t, s) \right\rangle \\ & \quad + \left\langle \mathcal{P}(t, \psi(t, s)) \frac{\partial \psi}{\partial s}(t, s), \frac{\partial}{\partial t} \mathcal{P}(t, \psi(t, s)) \frac{\partial \psi}{\partial s}(t, s) \right\rangle \quad (36) \\ & \leq -\Re \left\{ \left[\mathcal{P}(t, \psi(t, s)) \frac{\partial \psi}{\partial s}(t, s) \right]^H D^2 H(t, \psi(t, s)) \frac{\partial \psi}{\partial s}(t, s) \right\} \\ & \quad (37) \\ & \leq -c \Re \left\{ \left[\mathcal{P}(t, \psi(t, s)) \frac{\partial \psi}{\partial s}(t, s) \right]^H \mathbf{R}^{-1} \mathcal{P}(t, \psi(t, s)) \frac{\partial \psi}{\partial s}(t, s) \right\}. \end{aligned} \quad (38)$$

To obtain (34), we replaced $\frac{\partial}{\partial t} \frac{\partial \psi}{\partial s}(t, s)$ in the first term of the LHS by

$$\begin{aligned} \cdot & = \frac{\partial}{\partial s} \frac{\partial \psi}{\partial t}(t, s) = \frac{\partial}{\partial s} \mathbf{f}(t, \psi(t, s)) \\ & = \frac{\partial}{\partial \mathbf{x}} \mathbf{f}(t, \psi(t, s)) \frac{\partial \psi}{\partial s}(t, s) \\ & = \frac{\partial}{\partial \mathbf{x}} \frac{\partial}{\partial t} \psi(t, s) \frac{\partial \psi}{\partial s}(t, s). \end{aligned}$$

To obtain (35), we combined the last two terms in the LHS. The reasoning for the (in-) equalities (36), (37), and (38) are as follows. To obtain (36), the first term in (35) is simplified by substituting in

$$\begin{aligned} \mathcal{P}(t, \mathbf{x}) \dot{\mathbf{x}} & = \mathcal{P}(t, \mathbf{x}) [\mathbf{J}(t, \mathbf{x}) \nabla H(t, \mathbf{x}) - \mathbf{R} \nabla H(t, \mathbf{x})] \\ & = -\mathbf{R} \nabla H(t, \mathbf{x}), \end{aligned}$$

where the last equality is a consequence of the definition (15). In the LHS of (37), the second term is eliminated as follows. Note that, the integral of the second term over $s \in [0, 1]$,

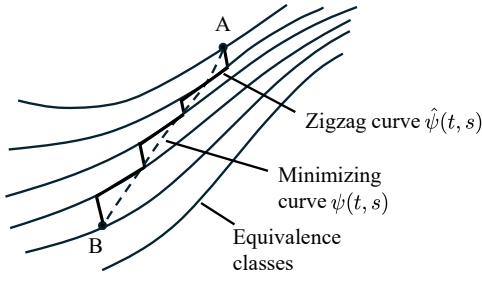


Fig. 5. Illustration of a key step in proving the contraction of the quotient distance: a zigzag approximation of the minimizing curve and to prove contraction of every transverse zigs.

can be approximated up to arbitrary accuracy with a series of zigzag curve segments $\hat{\psi}_i(t, s)$, $i = 1, \dots, N$ such that

$$\mathcal{P}(t, \hat{\psi}_i(t, s)) \frac{\partial \hat{\psi}_i}{\partial s}(t, s) = \begin{cases} \frac{\partial \hat{\psi}_i}{\partial s}(t, s) & \text{transverse zig} \\ 0 & \text{parallel zag} \end{cases}$$

The approximation is illustrated in Fig 5. Since $\mathcal{P}(t, \hat{\psi}_i(t, s))$ shrinks the transverse zigs for $t > t_0$, for the transverse zigs, we have that

$$\begin{aligned} & \left\langle \mathcal{P}(t, \hat{\psi}_i(t, s)) \frac{\partial \hat{\psi}_i}{\partial s}(t, s), \frac{\partial}{\partial t} \mathcal{P}(t, \hat{\psi}_i(t, s)) \frac{\partial \hat{\psi}_i}{\partial s}(t, s) \right\rangle \\ &= \left\langle \frac{\partial \hat{\psi}_i}{\partial s}(t, s), \frac{\partial}{\partial t} \mathcal{P}(t, \hat{\psi}_i(t, s)) \frac{\partial \hat{\psi}_i}{\partial s}(t, s) \right\rangle \leq 0, \end{aligned}$$

because any change in the projection $\mathcal{P}(t, \hat{\psi}_i(t, s))$ decreases the length of the zig segment, and, for the parallel zags,

$$\begin{aligned} & \left\langle \mathcal{P}(t, \hat{\psi}_i(t, s)) \frac{\partial \hat{\psi}_i}{\partial s}(t, s), \frac{\partial}{\partial t} \mathcal{P}(t, \hat{\psi}_i(t, s)) \frac{\partial \hat{\psi}_i}{\partial s}(t, s) \right\rangle \\ &= \left\langle 0_n, \frac{\partial}{\partial t} \mathcal{P}(t, \hat{\psi}_i(t, s)) \frac{\partial \hat{\psi}_i}{\partial s}(t, s) \right\rangle = 0 \end{aligned}$$

because $\mathcal{P}(t, \hat{\psi}_i(t, s)) \frac{\partial \hat{\psi}_i}{\partial s}(t, s) = 0_n$. To obtain (38), we used the same zigzag approximation and

$$c \lambda_{\max}(\mathbf{R}^{-1}) = \frac{c}{\lambda_{\min}(\mathbf{R})} = \lambda_{\min}(D^2 H(t, \mathbf{x})).$$

3. From steps 1 and 2, we have proved that, at $t = t_0$ and for a series of zigzag curve segments $\hat{\psi}_i(t, s)$, $1 = 1, \dots, N$ approximating the minimizing (at $t = t_0$) curve $\psi(t, s)$, the inequality (31) holds. Since as the number of zigzag curves segments N increases, both the LHS and the RHS of (31) converge to the minimum value. Hence (29) holds. \square

C. Proof of Proposition 2

Choose the inner product $\langle \mathbf{y}, \mathbf{x} \rangle = \Re\{\mathbf{y}^* \mathbf{x}\}$. The proof is otherwise the same as the proof of Proposition 1. \square

D. Proof of Proposition 3

From Proposition 1, we have that, for every initial condition (t_0, \mathbf{x}_0) , there is

$$\lim_{t \rightarrow \infty} \text{dist}(t, \Phi(t, t_0, \mathbf{x}_0), \bar{\mathbf{x}}(t)) = 0.$$

By property (iv) of the quotient distance that follows (16), it implies that

$$\lim_{t \rightarrow \infty} H(t, \Phi(t, t_0, \mathbf{x}_0) - H(t, \bar{\mathbf{x}}(t)) = 0.$$

This completes the proof. \square

E. Proof of Proposition 4

From Proposition 3, it suffices to show that there is a particular solution $\bar{\mathbf{x}}(t)$ such that

$$\frac{d}{dt} H(t, \bar{\mathbf{x}}(t)) = 0 \quad (39)$$

for all $t \in \mathbb{R}$. To this end, consider the set $E = E_t$ in which the Hamiltonian has zero derivative. By definition, E is an invariant set. Assume that the flow is complete. Then from any initial condition $(t_0, \mathbf{x}_0) \in \mathbb{R} \times E$, the solution $\bar{\mathbf{x}}(t) = \Phi(t, t_0, \mathbf{x}_0)$ satisfies (39). Hence we have found a particular solution, which completes the proof. \square

F. Proof of Lemma 1

We change to coordinates that are rotating at the frequency ω_0 by the change of variables

$$\mathbf{x} \leftarrow e^{-j\omega_0 t} \mathbf{x}.$$

The system equation then writes

$$\dot{\mathbf{x}} = (\mathbf{J}_1 - \mathbf{R}) \nabla H(\mathbf{x}) + \mathbf{G} u_1$$

where $u_1 = 1$ and $\mathbf{J}_1 = \mathbf{J} - j\omega_0 \mathbf{Q}^{-1}$. Now, consider the shifted Hamiltonian function

$$\mathcal{H}(\mathbf{x}, \bar{\mathbf{x}}(0)) = \frac{1}{2} [\mathbf{x} - \bar{\mathbf{x}}(0)]^H \mathbf{Q} [\mathbf{x} - \bar{\mathbf{x}}(0)].$$

It is easy to find its time derivative as [44]

$$\begin{aligned} \dot{\mathcal{H}}(\mathbf{x}, \bar{\mathbf{x}}(0)) &= -[\mathbf{x} - \bar{\mathbf{x}}(0)]^H \mathbf{Q} \mathbf{R} \mathbf{Q} [\mathbf{x} - \bar{\mathbf{x}}(0)] \\ &\leq -\lambda_{\min}(\mathbf{R}) \lambda_{\min}(\mathbf{Q}) \mathcal{H}(\mathbf{x}, \bar{\mathbf{x}}(0)). \end{aligned}$$

Hence

$$\begin{aligned} & \lim_{t \rightarrow \infty} \mathcal{H}(\mathbf{x}(t), \bar{\mathbf{x}}(0)) \\ &= \lim_{t \rightarrow \infty} \frac{1}{2} [\mathbf{x}(t) - \bar{\mathbf{x}}(0)]^H \mathbf{Q} [\mathbf{x}(t) - \bar{\mathbf{x}}(0)] = 0. \end{aligned}$$

Hence we obtain that the state vector \mathbf{x} converges to the limit cycle $\bar{\mathbf{x}}(0)$, and the orbit of the limit cycle is the limit set of all solutions. \square

G. Proof of Proposition 5

By Proposition 4, we obtain that the limit set of every solution is contained in the level set of $H(\mathbf{s}) = \frac{1}{2} \mathbf{s}^H \mathbf{Q}^{-1} \mathbf{s}$ occupied by $\bar{\mathbf{x}}(t)$, which is the first constraint we will use to characterize the limit set. We proceed to prove that the Hamiltonian of every edge satisfies the same property.

Consider a perturbation of the gradient of the Hamiltonian written as

$$\nabla \hat{H}(t, \mathbf{x}_1) = \mathbf{P}^{-1} \nabla H(t, \mathbf{x}_1)$$

where

$$\mathbf{P} = \text{diag}(p_1 \mathbf{I}_2, p_2 \mathbf{I}_2, p_3, p_4, p_5, p_6, p_7)$$

for $p_i > 0$, $i = 1, \dots, 7$. The overall pH system can then be written as

$$\dot{\mathbf{x}}_1 = (\mathbf{J}(\mathbf{x}) - \mathbf{R})\mathbf{P}\nabla\hat{H}(t, \mathbf{x}_1).$$

It can be checked that

$$\frac{1}{2} \left[(\mathbf{J}(\mathbf{x}) + \mathbf{R})\mathbf{P} + \mathbf{P}(\mathbf{J}(\mathbf{x}) + \mathbf{R})^H \right] \quad (40)$$

is a constant matrix, and (40) remains negative definite if we choose $\text{col}(p_i) \approx 17$. By Proposition 3, we have that the value of $\hat{H}(\mathbf{s})$ on the positive limit set should be equal to the value at $\bar{\mathbf{x}}(\tau)$. By choosing linearly independent $\text{col}(p_i)$'s we can fix the value of the Hamiltonian of every edge; that is, the voltage amplitude of every shunt capacitor, the current amplitude of every R–L line, and the energy stored in every SG are all equal to their values at $\bar{\mathbf{x}}(\tau)$.

To separate the Hamiltonian associated with the mechanical and the electrical energy of the SG, consider a perturbed system having a shunt capacitor that splits the stator inductance of each SG; that is, the subsystem (the subscript $i \in \{1, 2\}$ is omitted)

$$L\dot{I} = -RI - \psi j\omega e^{j\theta} + V$$

is replaced by

$$\begin{cases} \alpha L\dot{I}_1 = -\alpha RI_1 - \psi j\omega e^{j\theta} + V_1 \\ C\dot{V}_1 = -GV_1 + I_2 - I_1 \\ (1 - \alpha)L\dot{I}_2 = -(1 - \alpha)RI_2 - V_1 + V \end{cases}$$

where $0 < \alpha < 1$ and $C, G > 0$ are small. By Theorem 3.5 in [23], as α, C, G tend to zero, the solutions of the perturbed system tends to those of the original system. Applying the same contraction analysis to the perturbed system, we have that the mechanical energy $\frac{1}{2}J\omega_i^2$ and stator electrical energy $\frac{1}{2}L_i\|I_i\|^2$ are both equal to their value at the perturbed limit cycle. Taking the added shunt capacitance to zero, we obtain that the value of ω_i in the positive limit set of the original system is equal to the synchronized frequency of $\bar{\mathbf{x}}(\tau)$. The dynamics on the positive limit set is then constrained to be a passive RLC circuit with two voltage sources of the same frequency. By Lemma 1, the orbit of $\bar{\mathbf{x}}(\tau)$ is the only possible limit set. \square

REFERENCES

- [1] N. Hatziaargyriou, J. Milanovic, C. Rahmann, V. Ajjarapu, C. Canizares, I. Erlich, D. Hill, I. Hiskens, I. Kamwa, B. Pal *et al.*, "Definition and classification of power system stability—revisited & extended," *IEEE Transactions on Power Systems*, vol. 36, no. 4, pp. 3271–3281, 2020.
- [2] J. Dai, "Practical approaches to perform transient stability studies for industrial and commercial power systems," in *2024 IEEE/IAS 60th Industrial and Commercial Power Systems Technical Conference (I&CPS)*. IEEE, 2024, pp. 1–14.
- [3] P. K. Bera and C. Isik, "Identification of stable and unstable power swings using pattern recognition," in *2021 IEEE Green Technologies Conference (GreenTech)*. IEEE, 2021, pp. 286–291.
- [4] D. A. Tziouvaras and D. Hou, "Out-of-step protection fundamentals and advancements," in *57th Annual Conference for Protective Relay Engineers, 2004*. IEEE, 2004, pp. 282–307.
- [5] M. Mahmud, H. Pota, M. Aldeen, and M. Hossain, "Partial feedback linearizing excitation controller for multimachine power systems to improve transient stability," *IEEE Transactions on Power systems*, vol. 29, no. 2, pp. 561–571, 2013.

- [6] A. Bidram, A. Davoudi, F. L. Lewis, and J. M. Guerrero, "Distributed cooperative secondary control of microgrids using feedback linearization," *IEEE Transactions on Power Systems*, vol. 28, no. 3, pp. 3462–3470, 2013.
- [7] C. Spanias and I. Lestas, "A system reference frame approach for stability analysis and control of power grids," *IEEE Transactions on Power Systems*, vol. 34, no. 2, pp. 1105–1115, 2018.
- [8] Z. Siahhaan, E. Mallada, and S. Geng, "Decentralized stability criteria for grid-forming control in inverter-based power systems," in *2024 IEEE Power & Energy Society General Meeting (PESGM)*. IEEE, 2024, pp. 1–5.
- [9] S. Y. Caliskan and P. Tabuada, "Compositional transient stability analysis of multimachine power networks," *IEEE Transactions on Control of Network systems*, vol. 1, no. 1, pp. 4–14, 2014.
- [10] P. Varaiya, F. F. Wu, and R.-L. Chen, "Direct methods for transient stability analysis of power systems: Recent results," *Proceedings of the IEEE*, vol. 73, no. 12, pp. 1703–1715, 1985.
- [11] H.-D. Chiang, F. Wu, and P. Varaiya, "Foundations of direct methods for power system transient stability analysis," *IEEE Transactions on Circuits and systems*, vol. 34, no. 2, pp. 160–173, 1987.
- [12] D. Rimorov, X. Wang, I. Kamwa, and G. Joós, "An approach to constructing analytical energy function for synchronous generator models with subtransient dynamics," *IEEE Transactions on Power Systems*, vol. 33, no. 6, pp. 5958–5967, 2018.
- [13] H. Cheng, W. Huang, C. Shen, Y. Peng, Z. Shuai, and Z. J. Shen, "Transient voltage stability of paralleled synchronous and virtual synchronous generators with induction motor loads," *IEEE Transactions on Smart Grid*, vol. 12, no. 6, pp. 4983–4999, 2021.
- [14] J. Schiffer, D. Efimov, and R. Ortega, "Global synchronization analysis of droop-controlled microgrids—a multivariable cell structure approach," *Automatica*, vol. 109, p. 108550, 2019.
- [15] F. Forni and R. Sepulchre, "Differential analysis of nonlinear systems: revisiting the pendulum example," in *53rd IEEE Conference on Decision and Control*. IEEE, 2014, pp. 3848–3859.
- [16] J. Schiffer, R. Ortega, A. Astolfi, J. Raisch, and T. Sezi, "Conditions for stability of droop-controlled inverter-based microgrids," *Automatica*, vol. 50, no. 10, pp. 2457–2469, 2014.
- [17] R. Remmert, *Theory of complex functions*. Springer Science & Business Media, 1991, vol. 122.
- [18] F. Bullo and A. D. Lewis, *Geometric Control of Mechanical Systems*, ser. Texts in Applied Mathematics. New York-Heidelberg-Berlin: Springer Verlag, 2004, vol. 49.
- [19] E. D. Sontag, "Contractive systems with inputs," in *Perspectives in Mathematical System Theory, Control, and Signal Processing: A Festschrift in Honor of Yutaka Yamamoto on the Occasion of his 60th Birthday*. Springer, 2010, pp. 217–228.
- [20] J. W. Simpson-Porco and F. Bullo, "Contraction theory on Riemannian manifolds," *Systems & Control Letters*, vol. 65, pp. 74–80, 2014.
- [21] G. Söderlind, "The logarithmic norm. history and modern theory," *BIT Numerical Mathematics*, vol. 46, pp. 631–652, 2006.
- [22] A. Bressan, *Lecture notes on functional analysis*. American Mathematical Society, 2012.
- [23] H. K. Khalil, *Nonlinear systems; 3rd ed.* Upper Saddle River, NJ: Prentice-Hall, 2002.
- [24] J. C. Willems, "The behavioral approach to open and interconnected systems," *IEEE control systems magazine*, vol. 27, no. 6, pp. 46–99, 2007.
- [25] S. Fiaz, D. Zonetti, R. Ortega, J. M. Scherpen, and A. van der Schaft, "A port-Hamiltonian approach to power network modeling and analysis," *European Journal of Control*, vol. 19, no. 6, pp. 477–485, 2013.
- [26] N. Barabanov, R. Ortega, and A. Pyrkin, "On contraction of time-varying port-Hamiltonian systems," *Systems & Control Letters*, vol. 133, p. 104545, 2019.
- [27] A. Yaghmaei and M. J. Yazdanpanah, "Trajectory tracking for a class of contractive port Hamiltonian systems," *Automatica*, vol. 83, pp. 331–336, 2017.
- [28] —, "On contractive port-Hamiltonian systems with state-modulated interconnection and damping matrices," *IEEE Transactions on Automatic Control*, vol. 69, no. 1, pp. 622–628, 2023.
- [29] D. Bao, S.-S. Chern, and Z. Shen, *An introduction to Riemann-Finsler geometry*. Springer Science & Business Media, 2012, vol. 200.
- [30] F. Forni and R. Sepulchre, "A differential Lyapunov framework for contraction analysis," *IEEE Transactions on Automatic Control*, vol. 59, no. 3, pp. 614–628, 2014.
- [31] K. Krhač, B. Maschke, and A. van der Schaft, "Port-hamiltonian systems with energy and power ports," *IFAC-PapersOnLine*, vol. 58, no. 6, pp. 280–285, 2024.

- [32] P. Monshizadeh, J. E. Machado, R. Ortega, and A. van Der Schaft, "Power-controlled hamiltonian systems: Application to electrical systems with constant power loads," *Automatica*, vol. 109, p. 108527, 2019.
- [33] D. Xia and G. T. Heydt, "Harmonic power flow studies part i-formulation and solution," *IEEE Transactions on Power Apparatus and systems*, no. 6, pp. 1257–1265, 1982.
- [34] D. Groß, M. Colombino, J.-S. Brouillon, and F. Dörfler, "The effect of transmission-line dynamics on grid-forming dispatchable virtual oscillator control," *IEEE Transactions on Control of Network Systems*, vol. 6, no. 3, pp. 1148–1160, 2019.
- [35] I. Subotić, D. Groß, M. Colombino, and F. Dörfler, "A Lyapunov framework for nested dynamical systems on multiple time scales with application to converter-based power systems," *IEEE Transactions on Automatic Control*, vol. 66, no. 12, pp. 5909–5924, 2020.
- [36] D. Efimov, J. Schiffer, N. Barabanov, and R. Ortega, "A relaxed characterization of ISS for periodic systems with multiple invariant sets," *European Journal of Control*, vol. 37, pp. 1–7, 2017.
- [37] D. Efimov and J. Schiffer, "On boundedness of solutions of state periodic systems: a multivariable cell structure approach," *IEEE Transactions on Automatic Control*, vol. 64, no. 10, pp. 4094–4104, 2019.
- [38] C. J. O'Rourke, M. M. Qasim, M. R. Overlin, and J. L. Kirtley, "A geometric interpretation of reference frames and transformations: dq0, Clarke, and Park," *IEEE Transactions on Energy Conversion*, vol. 34, no. 4, pp. 2070–2083, 2019.
- [39] V. Vittal, J. D. McCalley, P. M. Anderson, and A. Fouad, *Power System Control and Stability*. John Wiley & Sons, 2019.
- [40] J. D. Watson, Y. Ojo, K. Laib, and I. Lestas, "A scalable control design for grid-forming inverters in microgrids," *IEEE Transactions on Smart Grid*, vol. 12, no. 6, pp. 4726–4739, 2021.
- [41] X. Jiang, C. M. Lagoa, D. Huang, and Y. Li, "A reference frame-based microgrid primary control for ensuring global convergence to a periodic orbit," *arXiv preprint arXiv:2408.00916*, 2024.
- [42] B. B. Johnson, S. V. Dhople, A. O. Hamadeh, and P. T. Krein, "Synchronization of nonlinear oscillators in an LTI electrical power network," *IEEE Transactions on Circuits and Systems I: Regular Papers*, vol. 61, no. 3, pp. 834–844, 2014.
- [43] D. Groß, C. Arghir, and F. Dörfler, "On the steady-state behavior of a nonlinear power system model," *Automatica*, vol. 90, pp. 248–254, 2018.
- [44] N. Monshizadeh, P. Monshizadeh, R. Ortega, and A. van der Schaft, "Conditions on shifted passivity of port-Hamiltonian systems," *Systems & Control Letters*, vol. 123, pp. 55–61, 2019.